

RESEARCH ARTICLE

10.1002/2016JD025500

Key Points:

- The wave number 1 asymmetric structure plays a dominant role in the westward deflection of Typhoon Jangmi
- The ventilation flow associated with the wave number 1 gyres is responsible for most of the westward motion component
- The accurate analyzed vortex-scale asymmetric structures with radar data assimilation are important for tropical cyclone track forecasting

Correspondence to:

M. Xue,
mxue@ou.edu

Citation:

Wang, M., M. Xue, and K. Zhao (2016), An investigation on how inner-core structures obtained through radar data assimilation affect track forecasting of typhoon Jangmi (2008) near Taiwan Island, *J. Geophys. Res. Atmos.*, *121*, 10,601–10,616, doi:10.1002/2016JD025500.

Received 12 JUN 2016

Accepted 6 SEP 2016

Accepted article online 10 SEP 2016

Published online 24 SEP 2016

An investigation on how inner-core structures obtained through radar data assimilation affect track forecasting of typhoon Jangmi (2008) near Taiwan Island

Mingjun Wang^{1,2}, Ming Xue^{1,2,3}, and Kun Zhao¹

¹Key Laboratory of Mesoscale Severe Weather/MOE and School of Atmospheric Science, Nanjing University, Nanjing, China, ²Center for Analysis and Prediction of Storms, Norman, Oklahoma, USA, ³School of Meteorology, University of Oklahoma, Norman, Oklahoma, USA

Abstract The impacts of radar data assimilation (DA) on the westward track deflection of Typhoon Jangmi (2008) near Taiwan Island and the deflection mechanism are investigated. Initial conditions from two data assimilation experiments with significant track forecast differences are analyzed and compared. The environmental, axisymmetric, wave number 1 to 3 asymmetric fields of the typhoon are decomposed by using vortex separation and Fourier decomposition methods. The components are selectively recomposed into new initial conditions that include different vortex-scale components to examine the impact of individual components on the track prediction. The wave number 1 asymmetric structure is found to play a dominant role in the westward deflection of Typhoon Jangmi, and the accurate analysis of this component with radar DA helps to improve the track forecast. The wave number 1 asymmetric circulation is manifested as a pair of cyclonic and anticyclonic gyres with well-defined ventilation flows through the inner-core region, which provides additional steering of the typhoon vortex. The layer-mean environmental steering flow and ventilation flow associated with the wave number 1 gyres are further calculated to quantitatively evaluate the impact of ventilation flow. The ventilation flow is shown to be responsible for most of the westward motion component, suggesting again its role in causing the westward track deflection of Typhoon Jangmi. The results also suggest the importance of analyzing vortex-scale asymmetric structures for accurate tropical cyclone track forecasting, especially when there is a significant track deflection.

1. Introduction

In recent years, Doppler weather radar observations of radial velocity (V_r) and/or radar reflectivity (Z) have been assimilated, either directly [e.g., Xiao *et al.*, 2007; Zhao and Jin, 2008; Xiao *et al.*, 2009; Zhang *et al.*, 2009; Zhao and Xue, 2009; Li *et al.*, 2012; Zhang *et al.*, 2012; Zhao *et al.*, 2012b; Dong and Xue, 2013] or indirectly [Zhao *et al.*, 2012a; Li *et al.*, 2013, 2014; Wang *et al.*, 2014], into high-resolution numerical models to improve the initial conditions and subsequent forecasts of tropical cyclones (TCs) using various assimilation methods. The results of these studies have shown that the direct assimilation of V_r , Z , or indirect assimilation of retrieved winds (e.g., using ground-based velocity track display [Lee *et al.*, 1999] or TC track radar echo by correlations (T-TREC) [Wang *et al.*, 2011] methods) have positive impacts on TC intensity, track, and precipitation forecasting.

The impact of radar data assimilation (DA) on TC forecast is generally attributed to the improved initial condition that captures the inner-core structures of TCs, which are otherwise not well observed. The assimilation of V_r and/or radar-retrieved winds helps to build up inner-core TC circulations, especially the axisymmetric structure, and thus directly improve TC intensity analysis and prediction [e.g., Zhao and Xue, 2009; Zhao *et al.*, 2012b; Dong and Xue, 2013]. In many of these studies, the assimilation of radar data also led to improvement to the forecasting of TC track, and such improvement is usually attributed to the more accurate representation of the intensity and structure in the initial condition, although most of the times the main attention is paid to the axisymmetric component of the analyzed TCs [e.g., Zhao and Xue, 2009; Li *et al.*, 2012; Zhao *et al.*, 2012a; Dong and Xue, 2013]. Exactly how the improved intensity and structure help improve the track forecasting, especially in more complex cases where track has significant variations, has, however, received little detailed analysis, at least not in the context of radar DA impact.

TC motion over the sea has been well studied. TC track is generally governed by three fundamental mechanisms; they are (1) advection of relative vorticity associated with the TC by environmental flow (the so-called

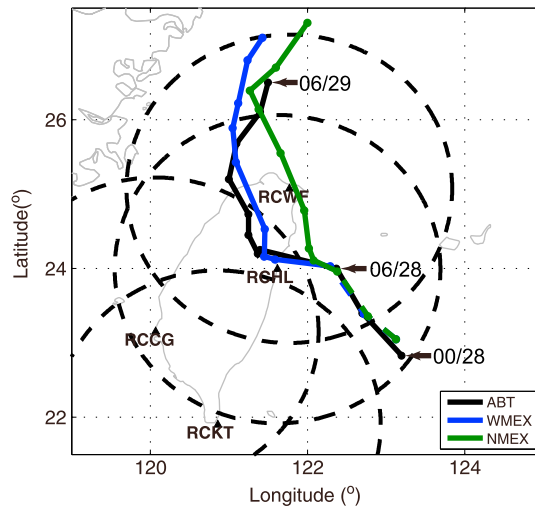


Figure 1. The tracks from 00:00 UTC on 28 September to 06:00 UTC on 29 September 2008 from experiments WMEX and NMEX, along with the average best track from 00:00 UTC on 28 September to 06:00 UTC on 29 September 2008. The dashed segments represent the track during assimilation cycles from 00:00 UTC to 06:00 UTC 28, while the solid segments indicate the track during forecast from 06:00 UTC on 28 September to 06:00 UTC on 29 September. The dots denote the center locations every 3 h.

et al., 2005; Peng *et al.*, 2012], and looping track prior to landfall [Jian and Wu, 2008; Yeh *et al.*, 2011]. Due to the modification of the background flow by the CMR, TCs approaching the northern (southern) part of the CMR tend to deflect to the north (south). Lin *et al.* [2005] pointed out the value of the vortex Froude number in determining if the TC track is continuous or discontinuous. Tang and Chan [2013] demonstrated that a pair of gyres are induced by the terrain and their associated flows near the TC center cause a northward deflection of the TC track prior to landfall. Jian and Wu [2008] and Huang *et al.* [2011] believe that the channeling effect occurring between the eastern side of the CMR and the approaching TC center plays an important role in the southward deflection and the subsequent looping track. Yeh *et al.* [2011] found that the interaction between the TC vortex and a cyclonic vortex induced over the southeastern part of Taiwan in a way similar to binary vortex interaction leads to the looping track of super Typhoon Haitang.

Studies cited above are mainly focused on the kinematic structures of TCs. Most recently, the impact of asymmetric latent heat distribution caused by precipitation asymmetry on TC track change has attracted significant attention [e.g., Wu and Wang, 2000; Chan *et al.*, 2002; C.-C Wang *et al.*, 2012; Hsu *et al.*, 2013; Wang *et al.*, 2013]. C.-C Wang *et al.* [2012] found that asymmetric latent heating associated with asymmetric precipitation along the CMR in Typhoon Morakot (2009) led to its slow motion upon leaving Taiwan. Wang *et al.* [2013] further showed that the asymmetric latent heating distribution caused the sudden and temporary motion speed reduction of Typhoon Fanapi (2010).

Most of these previous studies on the TC motion associated with terrain effects were based on numerical simulations. The initial conditions are either based on idealized typhoon vortices or from global model analyses, which usually do not contain realistic inner-core structure details. In other words, there is often limited direct evidence to verify the theories. Radar DA is a very effective way to “construct” the “true” state of TCs, especially for the inner-core structure, and thus potentially has the ability to reveal or verify the mechanisms responsible for observed TC track changes.

Typhoon Jangmi (2008) experienced complex track changes during its landfall over Taiwan. Jangmi made landfall on the east coast of Taiwan at 08:30 UTC on 28 September 2008. Before its landfall, Jangmi moved to the north-northwest, then deflected westward toward Taiwan at 06:00 UTC (Figure 1). The track turned northwestward after landfall, then north-northeastward after the center moved over Taiwan. Before and

steering flow); (2) advection processes (e.g., beta drift) that involve the interactions among the environmental flow, the planetary vorticity gradient, and the vortex circulation; and (3) the internal processes of the TC (such as the latent heating release) [e.g., Chan and Williams, 1987; Fiorino and Elsberry, 1989; Wu and Wang, 2000; Chan *et al.*, 2002]. When a TC approaches land, TC motion and the physical processes involved become more complex due to the interaction between the TC and terrain. Significant track deflection can occur, especially when coastal topography is high.

For relatively high topography such as the Central Mountain Range (CMR) of Taiwan, possible influences on TC track changes have been investigated extensively, including upstream deflection [e.g., Yeh and Elsberry, 1993a; Wu, 2001; Witcraft *et al.*, 2005], track discontinuity [e.g., Yeh and Elsberry, 1993b; Lin

during the landfall, Jangmi was observed by four operational S-band Doppler radars in Taiwan, from 00:00 UTC on 28 September to 00:00 UTC on 29 September.

For Typhoon Jangmi, Wang *et al.* [2014, 2016] assimilated Z and/or V_r data from up to four Doppler radars in Taiwan, or winds derived from reflectivity data by using the T-TREC method (referred to as V_{TREC} data) [Wang *et al.*, 2011] into a high-resolution numerical model using an ensemble Kalman filter (EnKF) near its landfall, and studied the impacts of the radar data assimilation on Jangmi's track, intensity, and precipitation forecasting. Wang *et al.* [2016] (hereafter W16) specifically examined the impacts of assimilating V_r versus V_{TREC} or their combinations and found that the track forecasts from different initial conditions had significant differences. The assimilation of V_{TREC} data in the first 30 min cycle and V_r data in the remaining cycles over the 6 h assimilation window gave the best track forecast, including capturing the leftward then rightward track deflection before and after landfall, respectively. The assimilation of V_{TREC} data throughout the 6 h window at 30 min intervals, however, produced a rather poor track forecast. Wang *et al.* [2016], like almost all aforementioned TC radar data assimilation studies, did not try to explain how the data assimilation affected the track forecasting, and in particular, what aspects of the analyzed TC initial condition led to improvement in the tracking forecasting, and how.

In this study, the initial conditions at 06:00 UTC on 28 September from the two experiments mentioned above are analyzed to help answer the above questions. The environmental, axisymmetric, wave number 1 to 3 asymmetric fields from those two initial conditions are decomposed and compared, and a series of forecasts from the recomposed initial conditions are performed to examine the impact of each of the components on the track forecast. The dominant component and the corresponding mechanism are further investigated based on the evolution of kinematic structures during the track deflection. The main goal of this paper is to answer how radar DA affects the track forecasting of Typhoon Jangmi, and to reveal the dominant mechanism governing the track deflection. It does not address any data assimilation issue, which is the topic of our earlier studies.

The rest of this paper is organized as follows. Section 2 describes the data sets from Wang *et al.* [2016] and the analysis methods used in this study. The impacts of different components of flow are examined in section 3. Section 4 presents the evolution of wave number 1 asymmetry and the corresponding mechanism governing the track deflection. Summary and discussions are presented in section 5.

2. Data, Methodology, and Experimental Design

2.1. Data Sets

Two radar data assimilation experiments, TFVR06 and TREC06, from W16 are chosen for our investigation, and they are renamed WMEX and NMEX in this study, indicating westward versus northward forecast tracks, respectively. In WMEX, the V_{TREC} winds retrieved from radar located at Hualian (RCHL in Figure 1) were assimilated in the first assimilation cycle at 00:00 UTC on 28 September by using the National Centers for Environmental Prediction operational Global Forecast System analysis as the background, and the V_r data from four Taiwan radars (triangles in Figure 1) were assimilated every 30 min from 00:30 through 06:00 UTC. In NMEX, the V_{TREC} data were assimilated from 00:00 UTC to 06:00 UTC every 30 min. No other type of data was assimilated. The Advanced Regional Prediction System (ARPS) [Xue *et al.*, 2000] was used as the prediction model with a physical domain of $2400 \times 2400 \times 25 \text{ km}^3$ and a 3 km horizontal grid spacing. The radar data were assimilated by using ARPS ensemble Kalman filter (EnKF) system. More details on the radar data and DA configurations and the experiments can be found in W16.

As discussed in W16, the V_{TREC} data are obtained through tracking radar reflectivity by correlation [Wang *et al.*, 2011] based on the assumption of conserved reflectivity advection. Being based on reflectivity data, which typically have a longer maximum measurement range than V_r data, V_{TREC} can provide larger spatial coverage, which is especially valuable when the TC is far away from ground-based radars. V_{TREC} data have lower resolutions ($\sim 10 \text{ km}$), however, than V_r data and can have significant error in the inner-core region [Tuttle and Gall, 1999; Wang *et al.*, 2011] or when reflectivity conservation is poorly satisfied. The latter can occur when Jangmi interacts with Taiwan terrain, triggering new convection [Tuttle and Gall, 1999; Wang *et al.*, 2011, 2016]. In comparison, V_r data have higher spatial resolutions, and when available from multiple

Doppler radars can provide detailed flow information. Due to the substantial differences between the V_r and V_{TREC} data, substantial differences were found in the forecast tracks of experiments WMEX and NMEX, as mentioned earlier.

The track forecasts of WMEX and NMEX are plotted in Figure 1, along with the average best track from three operational centers (W16). Jangmi moved to the north-northwest before landfall during 00:00 UTC–06:00 UTC, then deflected westward toward Taiwan at 06:00 UTC, and made landfall at about 08:30 UTC (Figure 1). The track turned northwestward after landfall, then turned north-northeastward after the center moved over Taiwan. The initial westward deflection close to landfall then northward turn after land is typical of many typhoons that passed over the Taiwan Island, and such turns were the subject of investigation in some of the aforementioned papers studying the effects of Taiwan Island on typhoon tracks.

Within the data assimilation window from 00:00 UTC to 06:00 UTC, both experiments capture well the north-northwestward motion (Figure 1). The track in WMEX captures well all three turns found in the best track, while the typhoon in NMEX turns north after a brief westward turn and barely makes landfall at the north corner of Taiwan. In another words, NMEX misses almost entirely the common-observed westward deflection, which would have led Jangmi to make landfall along the north-central coast of Taiwan Island. The only differences between WMEX and NMEX are with the initial conditions, which were obtained by assimilating different types of radar data. By comparing the initial conditions from WMEX and NMEX, we hope to be able to identify key features in the initial conditions causing the westward track deflection, and thereby better understand how the radar DA impacts typhoon track forecast in this case. Since WMEX predicts the track of Jangmi very accurately, we assume that its analyzed circulation is rather accurate, as far as the structures that affect its track over the next 24 h is concerned. By analyzing the flow structures associated with Jangmi during the landfall period, we hope to shed some light on the dominant physical process responsible for the westward deflection also.

2.2. Separation of Vortex and Environment

To examine the individual impact of the environmental steering flow and the vortex circulation on the track forecast, the environmental and vortex-scale fields are separated by using the technique proposed by Kurihara *et al.* [1993, 1995]. Details of the procedure can be found in Kurihara *et al.* [1995], except that the TC center is determined by using 850 hPa fields to reduce the influence of terrain. The Simplex method is employed to determine the TC center by maximizing the axisymmetric circulation [Nelder and Mead, 1965; Lee and Marks, 2000; M. Wang *et al.*, 2012]. The separation procedure is applied to the prognostic variables on the model levels of the ARPS, including the wind components (u , v , and w), potential temperature (θ), pressure (p), and water vapor mixing ratio (q_v). The track forecasting is not sensitive to the mixing ratios of hydrometeors in the initial condition (results not shown); thus, the mixing ratios of hydrometeors are not separated. This technique had been widely used in the TC bogus procedure for TC initialization [Kurihara *et al.*, 1993, 1995; Hsiao *et al.*, 2010], where the removal of the vortex from the background forecast is needed; therefore, the method is rather robust.

Figure 2 shows the total wind field, the separated environmental flow, and the vortex-scale circulation at 06:00 UTC on 28 September 2008 at model level 24 (~500 hPa) for WMEX and NMEX. It can be seen that the vortex circulation is quite successfully isolated from the environmental flow, with the vortex radius being about 650 km (Figures 2c and 2f). The environmental winds from NMEX and WMEX show similar patterns (Figures 2b and 2e), and the environmental flow crossing the TC center is mostly southerly (Figures 2b and 2e), which will act to steer the vortex northward. The differences in the environmental flows between NMEX and WMEX are generally less than 0.5 m s^{-1} (Figure 2h), suggesting nearly identical environmental flows in the two cases. The vortex circulation structures of NMEX and WMEX in the inner region (radius < 300 km) show substantial differences, which more or less exhibit a wave number 1 pattern with the maximum difference being over 15 m s^{-1} (Figures 2c, 2f, and 2i). In comparison, the differences are much smaller in the outer region, with the maximum difference being less than 4 m s^{-1} . The substantial differences in the inner region are mainly induced by the radar DA configurations, given that radar data coverage is mainly found in the inner region (see Figure 1). The similarity in environmental flows and difference in inner-core structures suggest that the inner-core vortex structures may play an important role on the westward deflection that occurs shortly after the initial condition time.

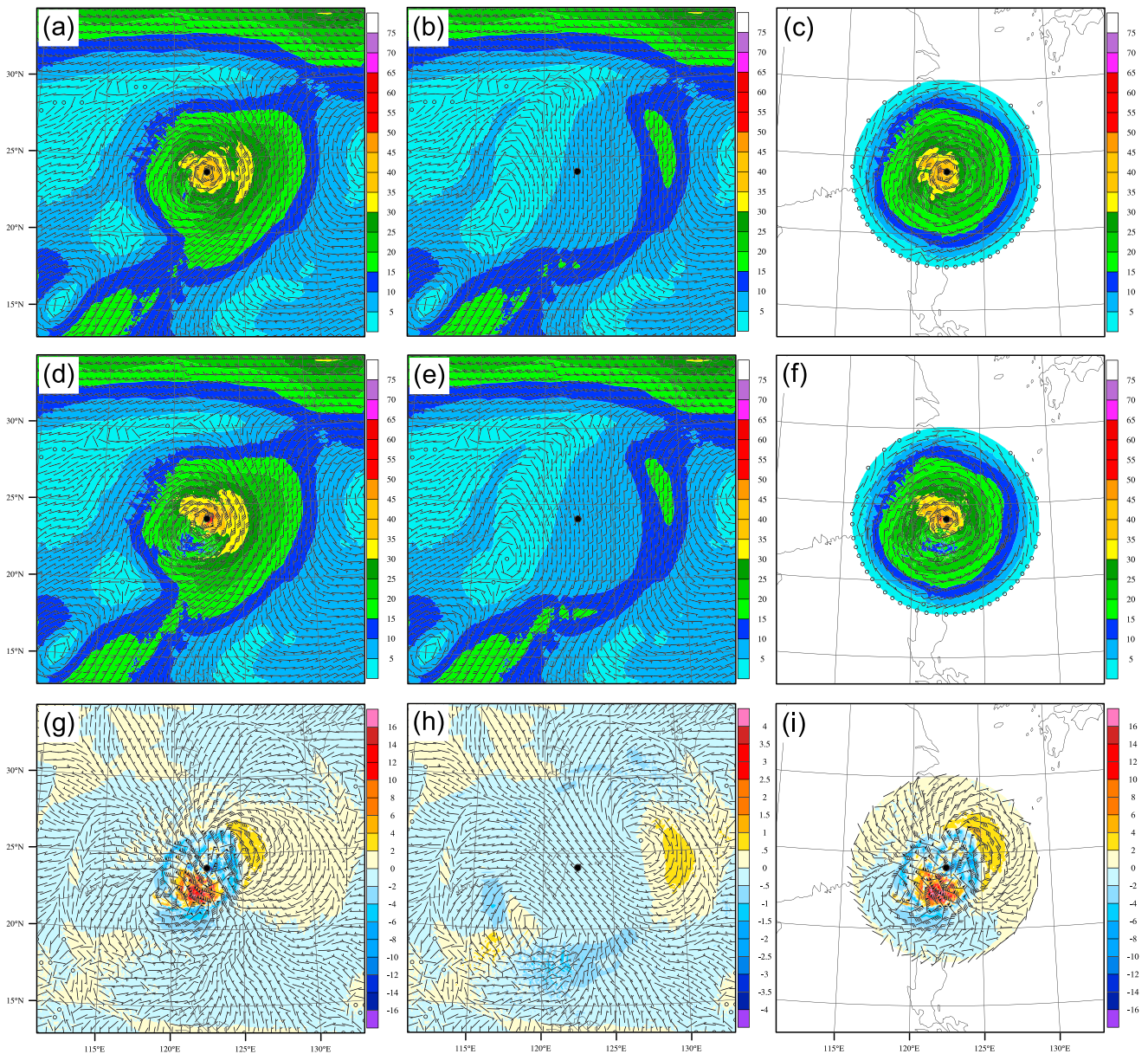


Figure 2. Separation of Typhoon Jangmi at 06:00 UTC 28 September 2008 at $k = 24$ (~500 hPa) for (a) total flow, (b) environment flow, and (c) typhoon vortex circulation from NMEC. (d–f) Same as Figures 2a–2c except from WMEX. (g–i) The differences of total flow, environment flow, and vortex circulation between NMEC and WMEX (NMEC-WMEX), respectively. The black dots indicate the observed typhoon center. The shading is the wind speed (m s^{-1}).

2.3. Fourier Decomposition

To better understand the differences in the vortices from NMEC and WMEX, including the axisymmetric and asymmetric structures and their impact on the track forecast [Marks et al., 1992; Tang and Chan, 2013], the extracted vortex-scale fields are further decomposed by using Fourier decomposition into azimuthal wave components, with our foci given to wave numbers (WNs) 0 through 3. Variables w , p , θ , and q_v are directly decomposed, while the tangential wind (V_T) and radial wind (V_R) components are first obtained by projecting the Cartesian wind components u and v onto the tangential and radial directions of the TC. All variables are interpolated into the cylindrical coordinates centered at the TC center, with an azimuthal resolution of 1° and a radial grid spacing of 3 km. The Fourier decomposition is performed at each radius, according to

$$X_r(k) = \sum_{n=1}^N x_r(n) \exp\left[\frac{-i2\pi(k-1)(n-1)}{N}\right] \quad 1 \leq k \leq N, \quad (1)$$

Table 1. Descriptions of Experiments

Experiments	Initial Condition
WMEX	The final analysis of V_{TREC} assimilation at 00:00 UTC and V_r assimilation from 00:30 UTC to 06:00 UTC
NMEX	The final analysis of V_{TREC} assimilation from 00:00 UTC to 06:00 UTC
WENV	Composed for the environment from WMEX and the vortex from NMEX
NEWV	Composed for the environment from NMEX and the vortex from WMEX
WMEXW0	As WMEX but only including wave number 0 vortex structures
NMEXW0	As NMEX but only including wave number 0 vortex structures
WMEXW1	As WMEX but only including wave number 0 + 1 vortex structure
WMEXW2	As WMEX but only including wave number 0 + 1 + 2 vortex structures
WMEXW3	As WMEX but only including wave number 0 + 1 + 2 + 3 vortex structures

where k represents the WN and $N = 360$ is the number of samples at each radius. The amplitude and phase of different WNs can be obtained for each radius as

$$A_r(k) = \sqrt{R[X_r(k)] + I[X_r(k)]}, \quad (2)$$

$$\varphi_r(k) = \text{atan}(R[X_r(k)], I[X_r(k)]), \quad (3)$$

where $R[\cdot]$ and $I[\cdot]$ represent the real and imagery parts, respectively. According to the amplitude and phase, the solution of each WN can be constructed as

$$\hat{X}_r(k) = A_r(k) \cos[\theta + \varphi_r(k)]. \quad (4)$$

After the decomposition in the cylindrical coordinate, fields associated with each WN component are interpolated back to the model grid, and V_T and V_R are transformed to u and v components. The axisymmetric (WN-0), and WN-1 through WN-3 components are obtained by applying the decomposition procedure at all model levels.

3. The Impact of Different Components on Typhoon Motion

A series of experiments is conducted by superimposing different components to form new initial conditions from which forecasts are launched, so as to examine the impact of individual components, including those of the environment, axisymmetric component, and WN-1 to WN-3 asymmetric components of the vortex (Table 1). In these experiments, the prognostic variables in the initial conditions, including u , v , w , θ , p , and q_v , are composed of the corresponding environmental and wave number components. To examine the relative impact of environmental and vortex-scale fields on the track forecast, the environmental fields from WMEX are exchanged with those from NMEX to form two new initial conditions, the corresponding forecast experiments are called NEWV (using NMEX's environment and WMEX's vortex) and WENV (using WMEX's environment and NMEX's vortex) (Table 1). The relative impacts of the axisymmetric structures are investigated through experiments WMEXW0 and NMEXW0, in which the asymmetric vortex structures (wave numbers above 0) are removed from the initial condition (retaining only the environment and WN-0) (Table 1). The impacts of asymmetric components are examined by including the environmental component and the vortex-scale structures with different number of waves in experiments WMEXW1, WMEXW2, and WMEXW3. In these experiments, the vortex-scale structures are composed of WN-0 through WN-1, WN-2, and WN-3, respectively. For instance, the initial condition of WMEXW3 included the environmental, WN-0, WN-1, WN-2, and WN-3 components. After the initial conditions are generated, 24 h forecasts are launched from 06:00 UTC on 28 September to 06:00 UTC on 29 September. The track forecasts are compared and carefully examined to reveal the dominant components in the initial condition that govern the track deflection. Since the initial conditions are directly affected by the wind DA, we mainly focus on the comparison and analyses of the flow structures from WMEX and NMEX.

3.1. The Impacts of Total Vortex Structure

The predicted tracks, track errors, minimum sea level pressure (MSLP), and maximum surface wind (MSW) from experiments WMEX, NMEX, WENV, and NEWV are plotted in Figure 3 along with the average best track. NEWV predicts well the westward motion of Jangmi and the two ensuing turns (Figure 3a) with the mean track error being about 50 km (Figure 3b), which is quite close to the track of WMEX. In contrast, WENV, similar

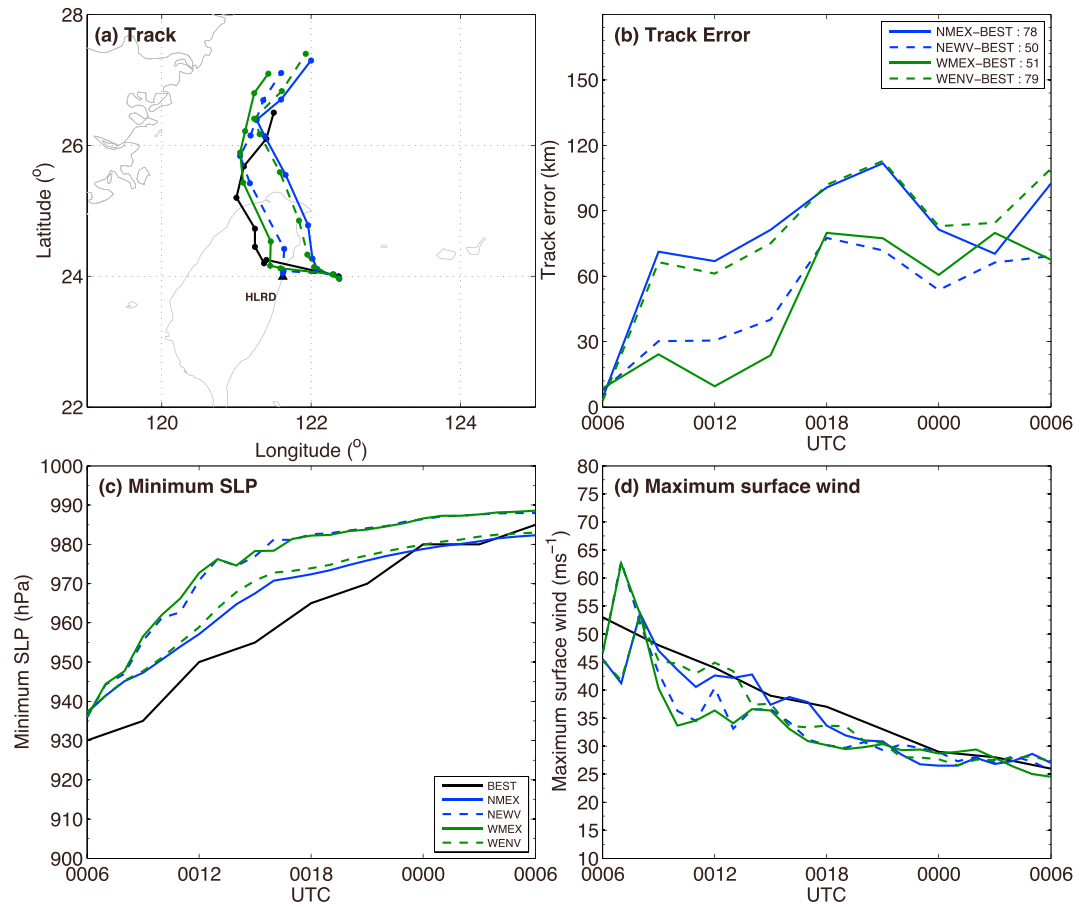


Figure 3. The predicted (a) tracks, (b) track errors, (c) minimum sea level pressures, and (d) maximum surface winds from 06:00 UTC on 28 September to 06:00 UTC on 29 September 2008, along with the average best track (ABT, see section 2). The dots in Figure 3a denote the center locations every 3 h starting from 06:00 UTC on 28 September. The numbers in Figure 3b denote the mean track errors over the forecast period against the ABT.

to NMEX, does not capture the westward motion and the correct landfall location, resulting in a significant eastward track bias and a mean track error of 79 km. Meanwhile, the predicted MSLPs and MSWs from NEWV (WENV) are similar to those from WMEX (NMEX) (Figures 3c and 3d). The similar track forecasts between NEWV and WMEX (WENV and NMEX) suggest that the differences in the environment fields from the two DA experiments have negligibly small effect on the westward track deflection, and in fact, the environmental differences from WMEX and NMEX are small (which are not significantly affected by the radar DA). The vortex-scale differences introduced by different radar DA in WMEX and NMEX lead to the track forecast differences, indicating the importance of accurately analyzing the vortex-scale structures in the TC initial conditions in this stage of forecast. Given the importance of the vortex-scale structures, we examine next different wave components of the vortex-scale circulation.

3.2. The Impacts of Axisymmetric Structures

The axisymmetric tangential winds (ATWs) in the initial conditions from WMEX and NMEX are first calculated and plotted in Figure 4. Axisymmetric radial winds are expected to have less effect on TC track and are therefore not shown. Both WMEX and NMEX have tight vortex circulations, with the radius of maximum wind at about 35 km. The axisymmetric circulation of WMEX (Figure 4a) is stronger than that of NMEX (Figure 4b), with the maximum ATW being over 50 m s^{-1} and the 45 m s^{-1} contour extending to 5.5 km height. The differences between WMEX and NMEX are mainly found within a radius of 300 km, while they are almost identical outside the radius of 300 km. This is because radar DA mainly affects the region within 300 km from TC center where most convection is found.

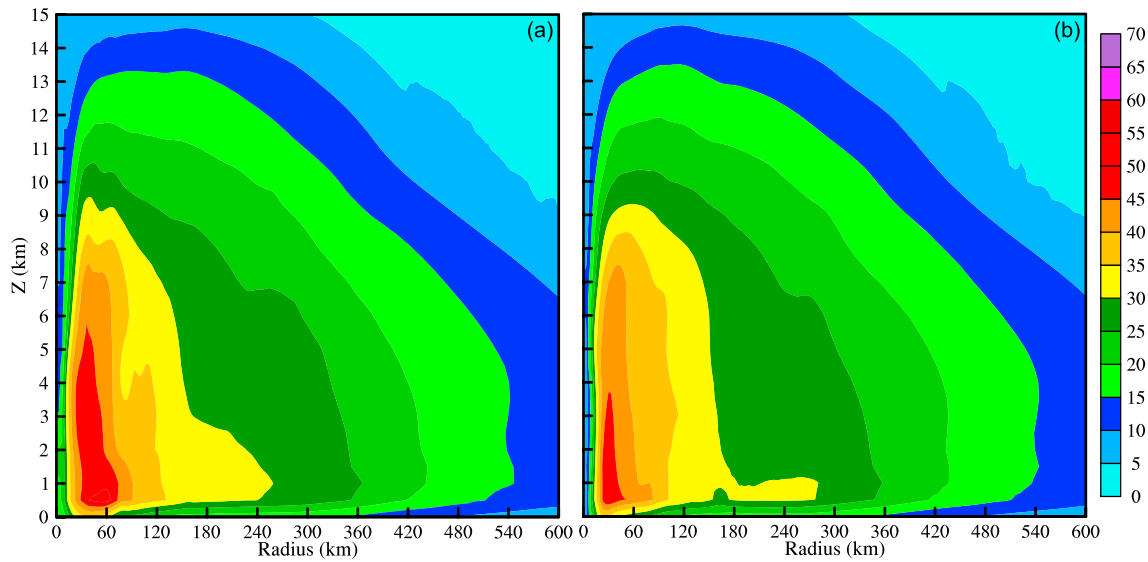


Figure 4. Azimuthally averaged tangential wind at 06:00 UTC 28 September 2008 from experiments (a) WMEX and (b) NMEX.

Figure 5 shows the predicted tracks and track errors from experiments WMEXW0 and NMEXW0, which include only the environmental and WN-0 components from the initial conditions of WMEX and NMEX, respectively. With only the axisymmetric structures, the predicted tracks of WMEXW0 and NMEXW0 are similar to each other; the predicted typhoon directly moves northward without westward deflection (Figure 5a), resulting in a mean track error of about 105 km (Figure 5b). This suggests that the axisymmetric structure is not responsible for the westward track deflection. Asymmetric structures are therefore likely the key in causing the westward deflection of Jangmi. The impacts of asymmetric components are examined next.

3.3. The Impacts of Asymmetric Structures

Figure 6 shows the asymmetric WN-1 through WN-3 winds at ~500 hPa from WMEX and NMEX. Both WMEX and NMEX show clear asymmetric structures, and the amplitudes of asymmetric structures decrease with increasing WN (Figure 6). The WN-1 component dominates the asymmetry in both cases, and it accounts for over 55% in terms of the asymmetry amplitude. Meanwhile, there are significant asymmetry differences between WMEX and NMEX in terms of amplitude and phase. The WN-1 circulation from WMEX shows a pair

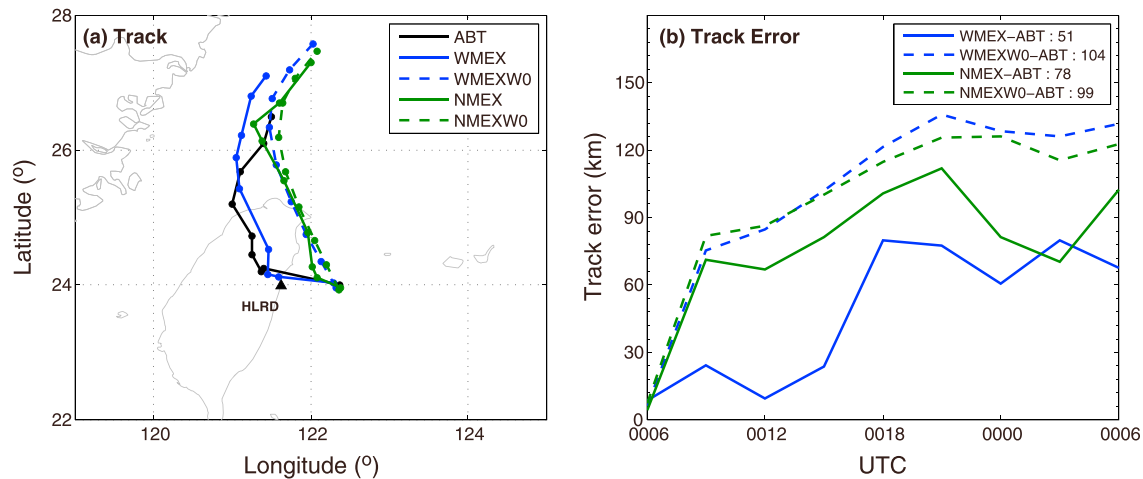


Figure 5. The predicted (a) tracks and (b) track errors from 06:00 UTC on 28 September to 06:00 UTC on 29 September 2008, along with the average best track (ABT, see section 2). The dots in Figure 5a denote the center locations every 3 h starting from 06:00 UTC on 28 September. The numbers in Figure 5b denote the mean track errors over the forecast period against the ABT.

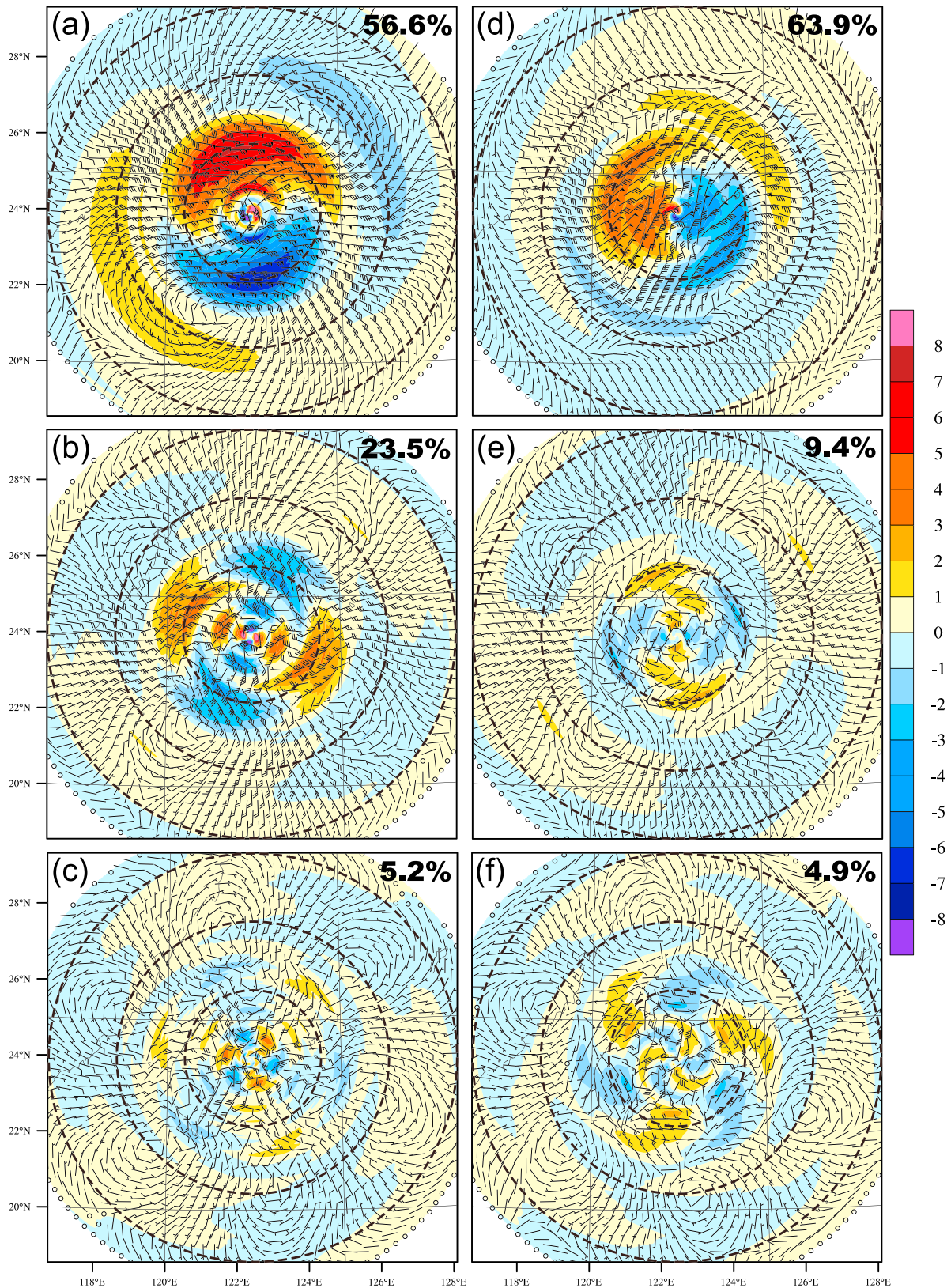


Figure 6. The Fourier decomposition of (a) wave number-1 component, (b) wave number-2 component, and (c) wave number-3 component from WMEX experiment at $k = 24$ (~500 hPa) at 06:00 UTC on 28 September 2008. (d–f) Same as Figures 6a–6c except from NMEX. The dashed circles indicate the range rings of 200 km, 400 km, and 600 km from the typhoon center. The number in each panel is the percentage of each wave number component in total asymmetry.

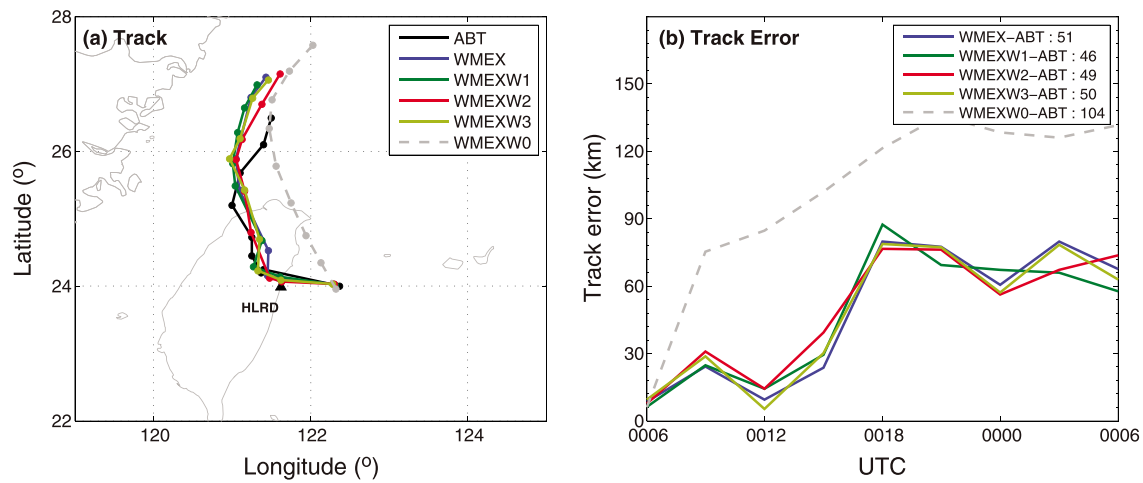


Figure 7. The predicted (a) tracks and (b) track errors from 06:00 UTC on 28 September to 06:00 UTC on 29 September 2008, along with the average best track (ABT, see section 2). The dots in Figure 7a denote the center locations every 3 h starting from 06:00 UTC on 28 September. The numbers in Figure 7b denote the mean track errors over the forecast period against the ABT.

of cyclonic and anticyclonic gyres, the cyclonic gyre to the southwest of Taiwan, and the anticyclonic gyre to the northeast of TC center (Figure 6a). Compared to WMEC, the cyclonic and anticyclonic gyres are located to the southeast and northwest of TC center (Figure 6d), indicating an almost 90° phase difference between WMEC and NMEX. The maximum wind speed of the WN-1 asymmetry is over 7 m s^{-1} , at the radius of $\sim 200 \text{ km}$ from TC center (Figure 6a). Compared to WMEC, the WN-1 asymmetry of NMEX is weaker, with the maximum wind speed of about 5 m s^{-1} found at the same radius (Figure 6d). Consistent with the WN-1 circulations, the maximum speed of NMEX is also 90° cyclonically shifted from the WN-1 structure of WMEC. The WN-2 and WN-3 asymmetries from NMEX are generally weaker than those of WMEC and also have relative phase shifts. The differences in the WN-1 to WN-3 asymmetries lead to the different track forecasts, as will be seen next.

Figure 7 shows the predicted tracks and track errors from WMECW1, WMECW2, and WMECW3, which include WN-0 through WN-1, WN-2, and WN-3, respectively, from WMEC, in addition to the environmental component. By including WN-1 in the initial condition but without WN-2 and above, WMECW1 is able to produce a similar track forecast as WMEC (Figure 7a), with a mean track error of 46 km that is close to that of WMEC (Figure 7b). Compared to WMECW0 containing only WN-0, the track forecast of WMECW1 is significantly improved, and the mean track error is reduced from 104 km to 46 km (Figure 7b). Further adding WN-2 and WN-3, the track forecasts of WMECW2 and WMECW3 do not change much from that of WMECW1, suggesting that WN-2 and WN-3 structures have very limited impact on the track forecasts here. The impacts of WN-1 through WN-3 components of NMEX are also tested; similar results are obtained (not shown). Clearly, the WN-1 asymmetry plays a dominant role in causing the westward track deflection, which affects the follow-on track forecast also. Apparently, the assimilation of V_r data from multiple radars in the later cycles in WMEC yields more accurate analysis of the asymmetric structure of Jangmi than the assimilation of V_{TREC} throughout the cycles in NMEX, and the asymmetric inner-core structures are found to be critical for accurate track forecasting of Jangmi near its landfall.

4. Evolution of WN-1 Circulation and the Ventilation Effect

The WN-1 asymmetric circulation is examined further in this section to understand how it affects the track forecasting. A careful examination of Figures 6a and 6d for the WN-1 structures reveals that there exists a clear, rather strong ventilation flow through the TC center between the cyclonic and anticyclonic gyres in both WMEC and NMEX cases at 06:00 UTC. The ventilation flow in WMEC is easterly (Figure 6a), which acts to translate the vortex westward and hence causes the westward deflection. In comparison, the ventilation flow in NMEX is mostly northerly (Figure 6d), which partially counteracts the impact of southerly environmental flow (see Figure 2b), and leads to a slower westward motion of the typhoon in NMEX (Figure 1).

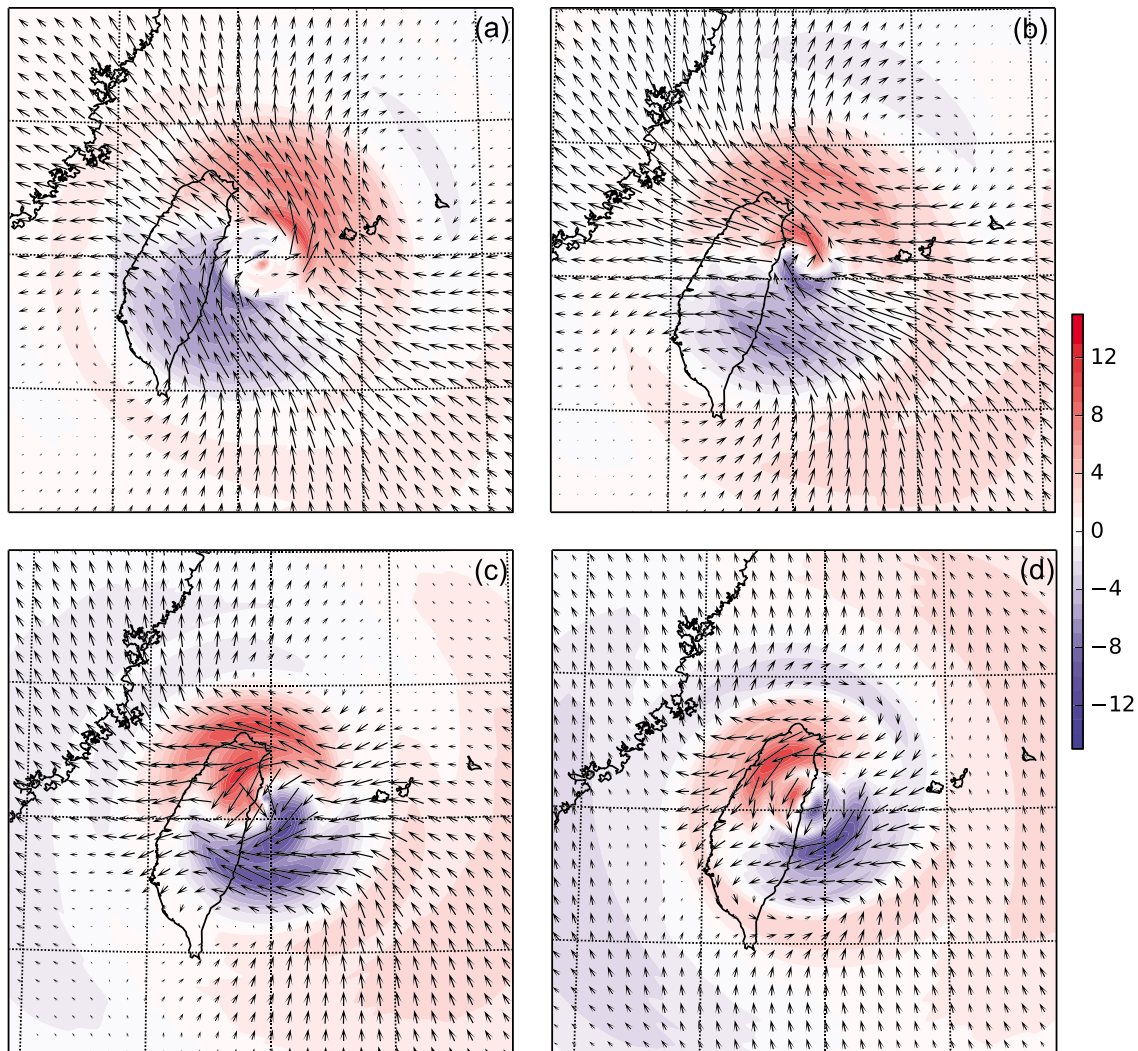


Figure 8. The evolution of wave number-1 circulation at 3 km height from 06:00 UTC to 09:00 UTC on 28 September 2008 in 1 hour interval for WMEX experiment.

Because WMEX predicts well Jangmi's track deflection, the evolution of its WN-1 structure is investigated in some details next, and the contribution of the associated ventilation flow to the westward track deflection is also evaluated.

4.1. Wavenumber-1 Structure Associated With the Typhoon Motion

Figure 8 shows the WN-1 circulation at the 3 km height from 06:00 UTC to 09:00 UTC on 28 September 2008 in 1 h intervals for WMEX. At 06:00 UTC (the initial time), the cyclonic and anticyclonic gyres are located east-northeast and west-southwest and about 300 km away from the TC center, respectively (Figure 8a). The corresponding WN-1 winds associated with the gyres have speeds of over 8 m s^{-1} . The ventilation flows through the TC inner-core region are mostly from the southeaster (except right at the TC center where wind direction from the Fourier decomposition has uncertainties), which translate the TC toward northwest (Figure 8a). One hour later, the gyres have been rotated around the TC center cyclonically somewhat (Figure 8b), and the cyclonic (anticyclonic) one is located more toward the east (west), and have gained some intensity and decreased in size than at 06:00 UTC. Accompanying the rotation of the gyres, the ventilation flows have become more easterly, therefore strengthening the westward flow and hence causing more westward deflection. By 08:00 UTC, half an hour before landfall, the gyres are located north-northeast and south-southwest of the TC center (Figure 8c), with the ventilation flow pointed southwest, which acts to steer the TC southwestward. After landfall (09:00 UTC), the gyres become weaker and closer to the TC center and

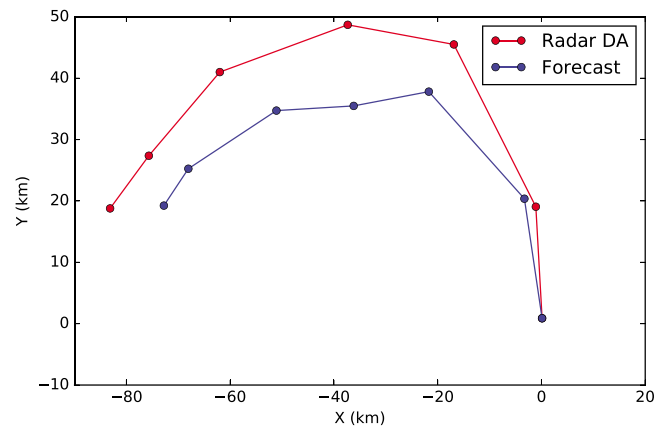


Figure 9. Averaged TC center between 2 to 6 km above ground for radar data assimilation (red line) and forecasts (blue line) from 06:00 UTC to 09:00 UTC in 30 min intervals.

are located at north-northwest and south-southeast of the TC center (Figure 8d). The broader ventilation flows still point toward southwest, but those near the TC center are mostly northerly. Overall, the WN-1 gyres rotate cyclonically and concentrate toward the TC center, apparently advected by the convergent vortex-scale circulations. Such signature is evident within the lower and middle levels, although only the circulation at 3 km is shown here to represent the evolution of the WN-1 structure and the ventilation flow. Layer-mean ventilation flows will be discussed in next section. The evolution of the asymmetric circulation of Jangmi in this study is actually similar to that in

Tang and Chan [2013], which studied the effects of cyclonic and anticyclone gyres in idealized simulations of typhoons. The gyres in their studies are generated through the interaction between the typhoon and the CMR of Taiwan [*Tang and Chan*, 2013, 2015b]. The induced gyres are advected by the symmetric flow of the TC and rotate cyclonically around the TC center according to their studies. Our results, in which the gyres are successfully analyzed by assimilating coastal radar data for a real case, support their findings, although we do not attempt to model the processing of typhoon-terrain interaction given the timing of our vortex initialization.

4.2. Ventilation Effects of Wavenumber-1 Circulation

To lend further support to our belief about the connection between WN-1 circulation and the track deflection, forecast track evolution in WMEX from 06:00 through 09:00 UTC at 30 min intervals is plotted in Figure 9 as blue line. Because there is no best track data every 30 min, radar V_r data assimilation is continued from 06:00 UTC through 09:00 UTC every 30 min with the same configurations as in WMEX to produce radar-based analyses of the best TC locations, and they are plotted in Figure 9 in red line for verification. The TC centers are determined from the analyzed wind fields by using the “Simplex” method by maximizing the axisymmetric circulation. Because the terrain-induced gyres mainly influence the lower and middle levels [*Tang and Chan*, 2013, 2015a, 2015b], the TC centers between 2 km and 6 km every 0.5 km are averaged to represent the track changes induced by the WN-1 gyres. Different from the relatively straight westward tracks as revealed by the track data at 3 h intervals seen earlier, the TC of WMEX actually moves northward during the first hour, then turns westward, and finally moves southwestward (Figure 9), creating a semicircle-like path. The TC in the analysis shows a similar track except for more northward and westward motion, indicating that the track change is well predicted by WMEX during the period of 06:00 to 09:00 UTC. The cyclonic curvature during this period is consistent with the cyclonically rotating WN-1 gyre pair, and the change in the direction of associated ventilation flow, further confirming the role of the WN-1 asymmetry in governing the westward deflection.

To be more quantitative, the low-to-mid-level mean environmental steering flow (SF) and the ventilation flow (VF) associated with the WN-1 circulation from 06:00 to 09:00 UTC at 1 h intervals are estimated and plotted in Figure 10, along with the motion vector (MV) of Jangmi. The steering flow is calculated by averaging the environmental flow every 0.5 km within the 2 to 6 km layer using a horizontal domain of 1200 km \times 1200 km centered on the typhoon after the vortex separation. The ventilation flow is defined as an area-average WN-1 circulation in the same vertical layer using a horizontal domain of 300 km \times 300 km centered on the typhoon. During the 3 h period, the steering flow does not change much and is southerly with a speed of about 5 m s⁻¹ (Figure 10). Consistent with the rotation of the WN-1 gyres, the mean ventilation flow rotates cyclonically during the 3 h forecast. At 06:00 UTC, the vector sum of SF and VF represents well the actual MV, with small speed and direction differences (Figure 10a). At 07:00 UTC, the VF turns more to the west and its westward component is almost the same as the MV (Figure 10b). However, the vector sum of SF and VF is pointed

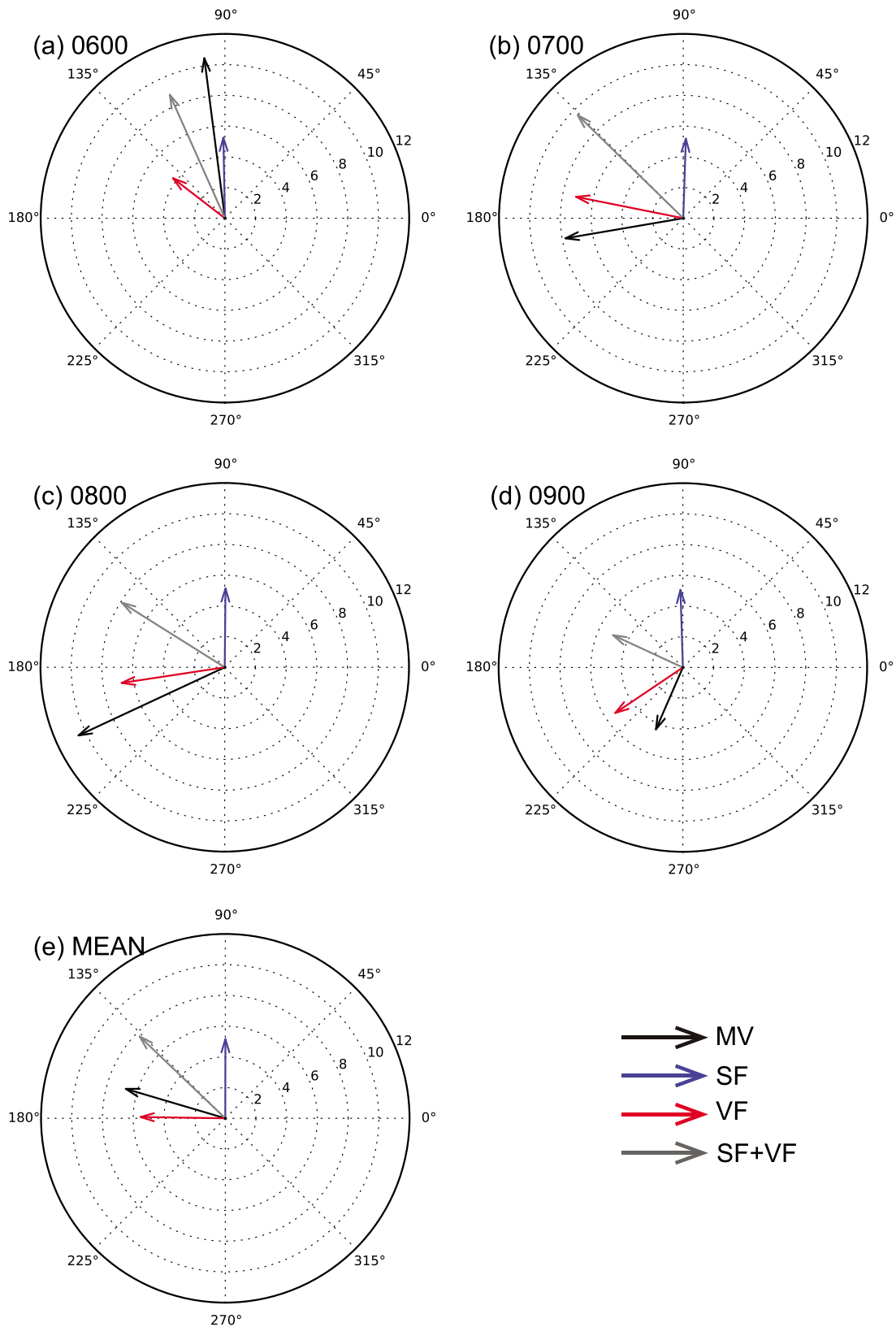


Figure 10. (a–d) The averaged motion vector (MV), steering flow (SF), and ventilation flow (VF) within 2 km to 6 km every 0.5 km from 06:00 UTC to 09:00 UTC in 1 hour interval, along with (e) the mean of the whole 3 h.

northwestward, suggesting that additional factors such as differential latent heating [C.-C Wang *et al.*, 2012; Hsu *et al.*, 2013; Wang *et al.*, 2013] might have provided additional southward steering of the TC. The westward component of VF is about 2 m s^{-1} weaker than the westward component of MV at 08:00 UTC (Figure 10c), while it is stronger at 09:00 UTC (Figure 10d). While the vector sum of SF and VF does not exactly match the actual MV of the typhoon, the tendency of the important contribution of VF is consistent with the cyclonic rotation of the MV vector during the above period. Without the correct representation of the WN-1 gyres, the track misses most of the westward turn and is apparently steered northward by the environmental flow, missing the land fall on the east coast of Taiwan.

The SF and VF during the 3 h period are further averaged and compared to the MV (Figure 10e). The vector sum of mean SF and VF is northwestward with about the same speed of 7 m s^{-1} as MV, while the direction difference is about 25° . The average ventilation flow is generally westward with a wind speed of about 6 m s^{-1} , which is $\sim 1 \text{ m s}^{-1}$ weaker than the westward component of MV. This suggests that the ventilation flow represents well the westward motion of Jangmi. Although there are still differences between the combination of SF and VF and the MV (especially in the south-north component), the role of VF in the westward deflection of Jangmi is clear. Overall, the WN-1 asymmetry, mostly likely induced by the Taiwan terrain, dominates the westward deflection of Typhoon Jangmi, and the ventilation flow associated with the WN-1 circulation provides most of the westward motion. Some remaining discrepancy can be due to asymmetric latent heating effects and the over-simplification of the mean flow vectors for steering the TC.

5. Summary and Discussion

Typhoon Jangmi (2008) experienced complex track changes before and after its landfall over the Taiwan Island. Before its landfall, Jangmi deflected from a north-northwest track to a westward track toward Taiwan at around 06:00 UTC 28 September 2008 and made landfall on the east coast of Taiwan at 08:30 UTC. Earlier, the observed radar reflectivity Z , radial velocity V_r , and the T-TREC (TC circulation tracking radar echo by correlation [Wang *et al.*, 2011]) retrieval winds (V_{TREC}) were assimilated into a high-resolution numerical model by using an ensemble Kalman filter (EnKF) to improve the initial condition and forecasting of Jangmi [Wang *et al.*, 2014, 2016]. Wang *et al.* [2016] (W16) examined the relative impacts of different assimilation configurations and found that the track forecasts from different initial conditions had significant differences. In this study, the impact of radar data assimilation on the track forecasting and the mechanism governing the track deflection of Jangmi are revealed by comparing the analyzed TC structures and the environmental flows in the initial conditions.

Based on W16, initial conditions from two data assimilation experiments, called TFVR06 and TREC06 in W16 (named WMEX and NMEX in this study), with significant track forecast differences are selected to perform detailed analyses. In WMEX, the westward deflection before landfall, northwestward, and then northward turns after landfall are all correctly predicted, while in NMEX, the westward deflection is mostly missed, caused the typhoon to miss most of the landfall.

The environmental, axisymmetric, asymmetric wave number-1 (WN-1) through WN-3 components in the final analyses or initial conditions of two experiments are decomposed by using a vortex separation technique and the Fourier decomposition method to isolate the impact of individual components on the prediction of the westward track deflection that is often observed of landfalling typhoon over Taiwan. Their impacts are investigated by conducting a series of 24 h forecast experiments, in which different components, including the environmental component, the axisymmetric component, and the WN-1 to WN-3 asymmetric components of vortex, are included in the initial conditions. Switching the environmental flow in the two experiments makes little difference. Including WN-1 only (excluding WN-1 and above) misses the westward deflection in both experiments. The inclusion of WN-1 makes key differences; the inclusion of the environmental flow and WN-0 and WN-1 from WMEX produced very similar track forecast as that of the original WMEX, while the inclusion of additional wave numbers produces little difference. The results suggest that it is critically important to accurately analyze the WN-1 component of TC circulation, via radar data assimilation. In this case, the assimilation of radial velocity produces more accurate analysis than assimilating T-TREC data in the later cycles.

The WN-1 circulation contains a prominent cyclonic-anticyclonic gyre pair. The gyres are believed to have been generated through the interaction between the TC vortex circulation and the Central Mountain

Range of Taiwan. These gyres are advected by the TC vortex circulation and rotate cyclonically around the TC center. The cyclonic curvature of the TC vortex track, both observed and model-predicted, during 06:00 UTC and 09:00 UTC is consistent with the cyclonic rotation of the WN-1 gyres, further confirming the role of the WN-1 asymmetry in causing the westward track deflection. Quantitative comparisons between the TC motion vector and the vector sum of the mean steering vector and mean ventilation vector also support the role of the WN-1 gyres and associated ventilation flow in the westward deflection process of Jangmi.

Tang and Chan [2013] found that a pair of terrain-induced gyres rotates cyclonically and the gyre-associated ventilation flow causes a northward deflection prior to landfall (~12 h before landfall) in their idealized simulations. However, significant westward advection is present right before the TC landfall (~3 h before landfall; their Figure 3), which is consistent with the gyre-induced ventilation flow found in this study within 3 h of the landfall. This study focuses on the kinematic asymmetric structures. However, the thermodynamic structures in a TC vortex can also have substantial impact on the track forecast. Wang *et al.* [2013] showed a southward component of TC motion caused by asymmetric diabatic heating before TC landfall over Taiwan, which may explain the missing southward motion component seen in our study when based on the steering flow and gyre-associated ventilation flow alone. Therefore, the ventilation flow associated with the wave number-1 gyre pair explains to a large extent the westward deflection of Jangmi's track toward the Taiwan Island, causing its landfall on the eastern coast. This study represents one of few studies, if any, that investigates and reveals how radar data assimilation and the improvement to the inner-core structures of a typhoon improves the subsequent track forecasting. Studies with more cases should be conducted to establish the generality of the results.

Acknowledgments

This work was primarily supported by the National 973 Fundamental Research Program of China (2013CB430103), the National Natural Science Foundation of China (grants 41605026, 41275031, and 41322032), and the DOD-ONR grant N00014-10-1-0775 and Social Common Wealth Research Program (GYHY201006007). The second author acknowledges the support of NSF grants AGS-0802888, AGS-1046171, and AGS-1261776. The data used in this study are available on a cloud drive. The url is <http://pan.baidu.com/s/1cyr6sm> with password xcxt.

References

- Chan, J. C. L., and R. T. Williams (1987), Analytical and numerical studies of the beta-effect in tropical cyclone motion. Part I: Zero mean flow, *J. Atmos. Sci.*, *44*(9), 1257–1265, doi:10.1175/1520-0469(1987)044<1257:aansot>2.0.co;2.
- Chan, J. C. L., F. M. F. Ko, and Y. M. Lei (2002), Relationship between potential vorticity tendency and tropical cyclone motion, *J. Atmos. Sci.*, *59*(8), 1317–1336, doi:10.1175/1520-0469(2002)059<1317:rbpvta>2.0.co;2.
- Dong, J., and M. Xue (2013), Assimilation of radial velocity and reflectivity data from coastal WSR-88D radars using an ensemble Kalman filter for the analysis and forecast of landfalling hurricane Ike (2008), *Q. J. R. Meteorol. Soc.*, *139*(671), 467–487, doi:10.1002/qj.1970.
- Fiorino, M., and R. L. Elsberry (1989), Some aspects of vortex structure related to tropical cyclone motion, *J. Atmos. Sci.*, *46*(7), 975–990, doi:10.1175/1520-0469(1989)046<0975:saovsr>2.0.co;2.
- Hsiao, L.-F., C.-S. Liou, T.-C. Yeh, Y.-R. Guo, D.-S. Chen, K.-N. Huang, C.-T. Terng, and J.-H. Chen (2010), A vortex relocation scheme for tropical cyclone initialization in advanced research WRF, *Mon. Weather Rev.*, *138*(8), 3298–3315, doi:10.1175/2010mwr3275.1.
- Hsu, L.-H., H.-C. Kuo, and R. G. Fovell (2013), On the geographic asymmetry of typhoon translation speed across the mountainous island of Taiwan, *J. Atmos. Sci.*, *70*(4), 1006–1022, doi:10.1175/JAS-D-12-0173.1.
- Huang, Y.-H., C.-C. Wu, and Y. Wang (2011), The influence of island topography on typhoon track deflection, *Mon. Weather Rev.*, *139*(6), 1708–1727, doi:10.1175/2011MWR3560.1.
- Jian, G.-J., and C.-C. Wu (2008), A numerical study of the track deflection of Supertyphoon Haitang (2005) prior to its landfall in Taiwan, *Mon. Weather Rev.*, *136*(2), 598–615, doi:10.1175/2007MWR2134.1.
- Kurihara, Y., M. A. Bender, and R. J. Ross (1993), An initialization scheme of hurricane models by vortex specification, *Mon. Weather Rev.*, *121*(7), 2030–2045, doi:10.1175/1520-0493(1993)121<2030:aisohm>2.0.co;2.
- Kurihara, Y., M. A. Bender, R. E. Tuleya, and R. J. Ross (1995), Improvements in the GFDL hurricane prediction system, *Mon. Weather Rev.*, *123*(9), 2791–2801, doi:10.1175/1520-0493(1995)123<2791:iitghp>2.0.co;2.
- Lee, W. C., and F. D. Marks (2000), Tropical cyclone kinematic structure retrieved from single-Doppler radar observations. Part II: The GBVTD-simplex center finding algorithm, *Mon. Weather Rev.*, *128*(6), 1925–1936, doi:10.1175/1520-0493(2000)128<1925:Tcksrfr>2.0.co;2.
- Lee, W.-C., B. J.-D. Jou, P.-L. Chang, and S.-M. Deng (1999), Tropical cyclone kinematic structure retrieved from single-Doppler radar observations. Part I: Interpretation of Doppler velocity patterns and the GBVTD technique, *Mon. Weather Rev.*, *127*(10), 2419–2439, doi:10.1175/1520-0493(1999)127<2419:TCKSRF>2.0.CO;2.
- Li, X., J. Ming, Y. Wang, K. Zhao, and M. Xue (2013), Assimilation of T-TREC-retrieved wind data with WRF 3DVAR for the short-term forecasting of typhoon Meranti (2010) near landfall, *J. Geophys. Res. Atmos.*, *118*, 10,361–10,375, doi:10.1002/jgrd.50815.
- Li, Y., X. Wang, and M. Xue (2012), Assimilation of radar radial velocity data with the WRF hybrid ensemble-3DVAR system for the prediction of Hurricane Ike (2008), *Mon. Weather Rev.*, *140*(11), 3507–3524, doi:10.1175/mwr-d-12-00043.1.
- Li, Z., Z. Pu, J. Sun, and W.-C. Lee (2014), Impacts of 4DVAR assimilation of airborne Doppler radar observations on numerical simulations of the Genesis of Typhoon Nuri (2008), *J. Appl. Meteorol. Climatol.*, *53*(10), 2325–2343, doi:10.1175/JAMC-D-14-0046.1.
- Lin, Y.-L., S.-Y. Chen, C. M. Hill, and C.-Y. Huang (2005), Control parameters for the influence of a mesoscale mountain range on cyclone track continuity and deflection, *J. Atmos. Sci.*, *62*(6), 1849–1866, doi:10.1175/JAS3439.1.
- Marks, F. D., R. A. Houze, and J. F. Gamache (1992), Dual-aircraft investigation of the inner core of Hurricane Norbert. Part I: Kinematic structure, *J. Atmos. Sci.*, *49*(11), 919–942, doi:10.1175/1520-0469(1992)049<0919:daioi>2.0.co;2.
- Nelder, J. A., and R. Mead (1965), A Simplex method for function minimization, *Comput. J.*, *7*(4), 308–313, doi:10.1093/comjnl/7.4.308.
- Peng, L., S. T. Wang, S. L. Shieh, M. D. Cheng, and T. C. Yeh (2012), Surface track discontinuity of tropical cyclones crossing Taiwan: A statistical study, *Mon. Weather Rev.*, *140*(1), 121–139, doi:10.1175/MWR-D-10-05050.1.
- Tang, C. K., and J. C. L. Chan (2013), Idealized simulations of the effect of Taiwan and Philippines topographies on tropical cyclone tracks, *Q. J. R. Meteorol. Soc.*, doi:10.1002/qj.2240.
- Tang, C. K., and J. C. L. Chan (2015a), Idealized simulations of the effect of local and remote topographies on tropical cyclone tracks, *Q. J. R. Meteorol. Soc.*, *141*(691), 2045–2056, doi:10.1002/qj.2498.

- Tang, C. K., and J. C. L. Chan (2015b), Idealized simulations of the effect of Taiwan topography on the tracks of tropical cyclones with different sizes, *Q. J. R. Meteorol. Soc.*, *142*, 793–804, doi:10.1002/qj.2681.
- Tuttle, J., and R. Gall (1999), A single-radar technique for estimating the winds in tropical cyclones, *Bull. Am. Meteorol. Soc.*, *80*(4), 653–668, doi:10.1175/1520-0477(1999)080<0653:asrtfe>2.0.co;2.
- Wang, C.-C., H.-C. Kuo, Y.-H. Chen, H.-L. Huang, C.-H. Chung, and K. Tsuboki (2012), Effects of asymmetric latent heating on typhoon movement crossing Taiwan: The case of Morakot (2009) with extreme rainfall, *J. Atmos. Sci.*, *69*(11), 3172–3196, doi:10.1175/JAS-D-11-0346.1.
- Wang, C.-C., Y.-H. Chen, H.-C. Kuo, and S.-Y. Huang (2013), Sensitivity of typhoon track to asymmetric latent heating/rainfall induced by Taiwan topography: A numerical study of Typhoon Fanapi (2010), *J. Geophys. Res. Atmos.*, *118*, 3292–3308, doi:10.1002/jgrd.50351.
- Wang, M., K. Zhao, and D. Wu (2011), The T-TREC technique for retrieving the winds of landfalling typhoons in China, *Acta Meteorol. Sin.*, *25*(1), 91–103, doi:10.1007/s13351-011-0007-x.
- Wang, M., K. Zhao, W.-C. Lee, B. J.-D. Jou, and M. Xue (2012), The Gradient Velocity Track Display (GrVTD) technique for retrieving tropical cyclone primary circulation from aliased velocities measured by single-Doppler radar, *J. Atmos. Oceanic Technol.*, *29*(8), 1026–1041, doi:10.1175/JTECH-D-11-00219.1.
- Wang, M., M. Xue, K. Zhao, and J. Dong (2014), Assimilation of T-TREC-retrieved winds from single-Doppler radar with an ensemble Kalman filter for the forecast of Typhoon Jangmi (2008), *Mon. Weather Rev.*, *142*(5), 1892–1907, doi:10.1175/MWR-D-13-00387.1.
- Wang, M., M. Xue, and K. Zhao (2016), The impact of T-TREC-retrieved wind and radial velocity data assimilation using EnKF and effects of assimilation window on the analysis and prediction of Typhoon Jangmi (2008), *J. Geophys. Res. Atmos.*, *121*, 259–277, doi:10.1002/2015JD024001.
- Witcraft, N. C., Y.-L. Lin, and Y.-H. Kuo (2005), Dynamics of orographic rain associated with the passage of a tropical cyclone over a mesoscale mountain, *Terr. Atmos. Oceanic Sci.*, *16*, 1133–1161.
- Wu, C.-C. (2001), Numerical simulation of Typhoon Gladys (1994) and its interaction with Taiwan terrain using the GFDL hurricane model, *Mon. Weather Rev.*, *129*(6), 1533–1549, doi:10.1175/1520-0493(2001)129<1533:NSOTGA>2.0.CO;2.
- Wu, L., and B. Wang (2000), A potential vorticity tendency diagnostic approach for tropical cyclone motion, *Mon. Weather Rev.*, *128*(6), 1899–1911, doi:10.1175/1520-0493(2000)128<1899:APVTDA>2.0.CO;2.
- Xiao, Q., Y.-H. Kuo, J. Sun, W.-C. Lee, D. M. Barker, and E. Lim (2007), An approach of radar reflectivity data assimilation and its assessment with the inland QPF of Typhoon Rusa (2002) at landfall, *J. Appl. Meteorol. Climatol.*, *46*(1), 14–22, doi:10.1175/jam2439.1.
- Xiao, Q., X. Zhang, C. Davis, J. Tuttle, G. Holland, and P. J. Fitzpatrick (2009), Experiments of hurricane initialization with airborne Doppler radar data for the advanced research hurricane WRF (AHW) model, *Mon. Weather Rev.*, *137*(9), 2758–2777, doi:10.1175/2009MWR2828.1.
- Xue, M., K. K. Droegemeier, and V. Wong (2000), The Advanced Regional Prediction System (ARPS)—A multi-scale nonhydrostatic atmospheric simulation and prediction model. Part I: Model dynamics and verification, *Meteorol. Atmos. Phys.*, *75*(3–4), 161–193, doi:10.1007/s007030070003.
- Yeh, T.-C., and R. L. Elsberry (1993a), Interaction of typhoons with the Taiwan orography. Part I: Upstream track deflections, *Mon. Weather Rev.*, *121*(12), 3193–3212, doi:10.1175/1520-0493(1993)121<3193:IOTWTT>2.0.CO;2.
- Yeh, T.-C., and R. L. Elsberry (1993b), Interaction of typhoons with the Taiwan orography. Part II: Continuous and discontinuous tracks across the island, *Mon. Weather Rev.*, *121*(12), 3213–3233, doi:10.1175/1520-0493(1993)121<3213:IOTWTT>2.0.CO;2.
- Yeh, T.-C., L.-F. Hsiao, D.-S. Chen, and K.-N. Huang (2011), A study on terrain-induced tropical cyclone looping in East Taiwan: Case study of Typhoon Haitang in 2005, *Nat. Hazards*, *63*(3), 1497–1514, doi:10.1007/s11069-011-9876-7.
- Zhang, F., Y. Weng, J. A. Sippel, Z. Meng, and C. H. Bishop (2009), Cloud-resolving hurricane initialization and prediction through assimilation of Doppler radar observations with an ensemble Kalman filter, *Mon. Weather Rev.*, *137*(7), 2105–2125, doi:10.1175/2009mwr2645.1.
- Zhang, L., Z. Pu, W.-C. Lee, and Q. Zhao (2012), The influence of airborne Doppler radar data quality on numerical simulations of a tropical cyclone, *Weather Forecast.*, *27*(1), 231–239, doi:10.1175/WAF-D-11-00028.1.
- Zhao, K., and M. Xue (2009), Assimilation of coastal Doppler radar data with the ARPS 3DVAR and cloud analysis for the prediction of Hurricane Ike (2008), *Geophys. Res. Lett.*, *36*, L12803, doi:10.1029/2009GL038658.
- Zhao, K., M. Xue, and W.-C. Lee (2012a), Assimilation of GBVTD-retrieved winds from single-Doppler radar for short-term forecasting of super typhoon Saomai (0608) at landfall, *Q. J. R. Meteorol. Soc.*, *138*(665), 1055–1071, doi:10.1002/qj.975.
- Zhao, K., X. Li, M. Xue, B. J.-D. Jou, and W.-C. Lee (2012b), Short-term forecasting through intermittent assimilation of data from Taiwan and mainland China coastal radars for Typhoon Meranti (2010) at landfall, *J. Geophys. Res.*, *117*, D06108, doi:10.1029/2011JD017109.
- Zhao, Q., and Y. Jin (2008), High-resolution radar data assimilation for Hurricane Isabel (2003) at landfall, *Bull. Am. Meteorol. Soc.*, *89*(9), 1355–1372, doi:10.1175/2008bams2562.1.